Available online at www.sciencedirect.com
ScienceDirect
Ceramics International 38 (2012) 801–809
CERAMICS INTERNATIONAL
www.elsevier.com/locate/ceramint

Investigation of AlF_3 doped ZnO thin films prepared by RF magnetron sputtering

Boen Houng *, Han Bin Chen

Department of Materials Science and Engineering, I-Shou University, Kaohsiung City 840, Taiwan, ROC

Received 11 July 2011; received in revised form 1 August 2011; accepted 2 August 2011
Available online 12th August 2011

Abstract

Transparent conducting ZnO thin films co-doped with aluminium and fluorine (AZO:F) were produced on glass substrates by RF magnetron sputtering at room temperature. The chemical AlF_3 was selected as a dopant, which allowed Al and F elements to be simultaneously substituted into sub-lattices sites of Zn and O, respectively. The microstructure, electrical and optical properties of ZnO thin films as a function of AlF_3 concentration were evaluated and compared to the films doped with Al_2O_3. From XRD analysis, it was revealed that the favoured orientation of ZnO films shifted from (0 0 2) to (1 0 3) as the amount of AlF_3 increased from 1 to 7 wt%. The film doped with 2 wt% AlF_3 showed improved crystallinity and a microstructure with larger, pyramid-like grains that were 120 nm long and 50 nm wide. As a result, the electrical resistivity of the AZO:F films had a minimum of $5.2 \times 10^{-4}\ \Omega$ cm. The improvement in the electrical resistivity of AZO:F films was due to the increase in carrier concentration from 7.0×10^{20} to $1.25 \times 10^{21}\ cm^{-3}$ and the mobility from 4.7 to 9.3 $cm^2\ V^{-1}\ s^{-1}$. Meanwhile, the electrical resistivity of the ZnO film doped with AlF_3 was found to be lower than that of the Al_2O_3-doped film. This was mainly attributed to the increase in carrier concentration by substituting Al and F atoms into the Zn and O sub-lattice sites, respectively, despite the slight decrease in the mobility. This increase in carrier concentration was also found to affect the optical property of the films due to the Moss–Burstein shift.

Keywords: ZnO thin films; Magnetron sputter; Carrier concentration; Electrical resistivity

1. Introduction

Zinc oxide (ZnO) has emerged to be one of the most promising oxide materials because of its numerous technological applications. For example, it can be used in gas sensors [1], varistors [2], surface acoustic wave devices [3], optical wave guides [4] and blue/UV light emitting devices [5]. Recently, ZnO has been considered as an excellent candidate to replace indium tin oxide (ITO) and tin oxide (SnO_2) as transparent conductive electrodes in flat panel display and solar cell devices [6–8]. The advantages of ZnO include its inexpensiveness and the relative ease of lithography. However, the electrical conductivity of un-doped zinc oxide is not high enough for practical application. Further reduction of ZnO resistivity can be achieved either by doping it with group III elements, such as B, Al, In and Ga to replace zinc atoms [9], or with group IV elements, such as F, to substitute oxygen atoms [10].

Electrical resistivity (ρ) depends on the carrier concentration (n) and mobility (μ) according to the relationship $1/\rho = ne\mu$, where, e is the electron charge. Obtaining high conductivity in the films is a trade-off between the carrier concentration and mobility because the relationship between the carrier concentration and mobility is governed by the rule $\mu \propto n^{-2/3}$ [11,12]. The highest reported room temperature Hall mobilities of heavily doped ZnO films are approximately 39 $cm^2\ V^{-1}\ s^{-1}$, which are limited by ionised impurity scattering [13]. Further increase of the mobility to 200 $cm^2\ V^{-1}\ s^{-1}$ can be achieved through improving the crystallinity of the tin films by preparing single crystal or hetero-epitaxial ZnO films [14]. Another way to improve the mobility is to modulate doping through multilayers of heavily and poorly doped semiconducting films [15,16]. However, data on heavily doped single crystal or epitaxial layers are rare, and the doping relies on advanced deposition techniques and facilities. Therefore, most research efforts have been focused on increasing the effective number of free carriers through

* Corresponding author. Tel.: +886 76579708; fax: +886 76578444.
E-mail address: boyen@mail.isu.edu.tw (B. Houng).

0272-8842/$36.00
doi:10.1016/j.ceramint.2011.08.007

impurity doping despite the physical upper limit of carrier concentration at approximately 1.5×10^{21} cm^{-3} [17]. Single elements, e.g., Al, Ga, In, B and F, are the most commonly used doping agents in ZnO films, and they have been evaluated in a few literatures [9,10,12]. However, the resistivity and mobility data are rather scattered and inconsistently reported in the literature. In addition, the optimal chemical and physical properties of current ZnO transparent conducting thin film have not been reached. Nevertheless, new and complex TCO materials are being explored to achieve this goal [18,19]. For example, co-doping of two elements in ZnO films, such as Al and Ru, Al and Co, Al and Mn, Al and V, and Al and F, has recently been undertaken to optimise the properties of the films for specialised applications [20–24]. The aim of this work is to investigate the properties of ZnO thin films doped with AlF_3. The chemical AlF_3 has not been selected as dopant source to produce n-type semiconducting ZnO films in previous works. It provided double doping effects in which the cationic Al^{3+} substitutes the Zn^{2+} ions, and the anionic F^{1-} substitutes O^{2-} ions in the ZnO crystal lattice. The influence of varying AlF_3 concentration on the microstructure, electrical and optical properties of ZnO thin films was presented in this work. For comparative purposes, Al_2O_3-doped ZnO thin films were prepared, and their properties were also determined.

2. Experimental procedures

ZnO films doped with aluminium and fluorine were produced by RF magnetron sputtering on glass substrates (Corning 1373) at room temperature. A mixture of ZnO (Aldrich, 99.99%) and AlF_3 (Aldrich, 99.99%) powders was sintered as the target for deposition at 1200 °C for 4 h. The AlF_3 doping concentrations were varied from 1 to 7 wt%. The distance between the target and the substrate was 8 cm. The vacuum chamber was first evacuated to a pressure of 10^{-6} Torr prior to deposition. The sputtering processes were carried out at a gas pressure of 3 m Torr in a pure argon atmosphere, and the RF power was set to 70 W. The sputtering time was 30 min and the resulting thickness was approximately 780 ± 15 nm.

An X-ray diffractometer (Panalyical, X'pert Pro) with Cu Kα radiation ($\lambda = 0.1542$ nm) was used for crystal structure evaluation. The surface microstructure and the morphology of the films were characterised by field emission scanning electron the microscopy (FESEM, Philips, XL-40FEG), atomic force microscopy (AFM, NaniMan NS4 D3100) and transmission electron microscopy (TEM, FEI, Tecnai G^2). The resistivity was measured with the Van der Pauw method. Optical transmittance measurements were carried out in the wavelength range of 300–900 nm using a UV/double-beam spectrophotometer.

3. Results and discussion

3.1. Microstructure and composition characterisations

The crystal structure of ZnO films co-doped with Al and F and prepared on glass substrates was examined by XRD measurements. Fig. 1 shows X-ray diffraction patterns of the ZnO films produced at room temperatures with AlF_3 concentration varying from 1 to 7 wt%. XRD patterns of these films did not show any appreciable changes from those of pure ZnO films. All samples in this work were genuine polycrystals with a wurtzite structure, and no other crystal phases were found. Meanwhile, the preferred crystallographic orientation shifted from (0 0 2) to (1 0 3) as the AlF_3 concentration increased from 1 to 7 wt%. The intensity of the *c*-axial (0 0 2) peak increased as the AlF_3 content increased to 2 wt% and decreased as the AlF_3 content continued to increase. On other hand, the intensity of the (1 0 3) diffraction peak increased with the AlF_3 content and dominated as the preferred orientation at in the films doped with 7 wt% AlF_3. The formation of the preferred orientation in the thin films is governed by the surface energy of the crystal plane. Moreover, the surface energy for the compound semiconductors depends strongly on the hybridised orbit [25]. In general, materials with a hexagonal structure (such as ZnO) tends to grow along the plane with the lowest surface energy, (which was [0 0 2] in this case), where the sp^3 hybridised orbits were direct spread. Aita et al. has also pointed out that the highly oriented [0 0 2] films can be obtained, if the Zn-to-ZnO ion ratio was minimised in a plasma atmosphere during sputtering [26]. In this work, the preferred crystallographic orientation shifted from (0 0 2) to (1 0 3) could be explained by changing the surface energy of ZnO crystal. The bonding energy of F–Zn (88 kcal/mol) is larger than that of the O–Zn bond (67.9 kcal/mol) [27], then the formation of Zn–F molecules is more stable than the formation of Zn–O molecules. Hence, as AlF_3 content increased, the Zn–F increased and then a growth competition between ZnF_2 and ZnO took place. Nevertheless, an increase in Zn-to-ZnO ion ratio could be attained during sputtering and thus the preferred orientation was not occurred along (0 0 2) instead of (1 0 3).

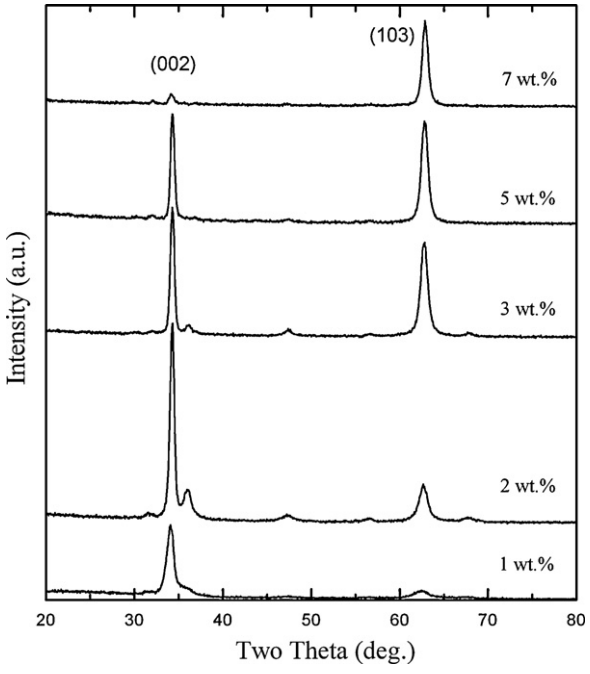

Fig. 1. X-ray diffraction patterns of ZnO films doped at different AlF_3 concentrations.

The change in preferred crystallographic orientation of ZnO films as a function of ammonium fluoride doping was also found in preparing ZnO films by chemical spray method [28].

The effect of the AlF_3 dopant concentration on the crystallinity and crystal size of ZnO films was determined according to the Scherrer formula [29]

$$D = \frac{0.94\lambda}{\mathrm{FWHM}\cos\theta} \quad (1)$$

where D is the crystal size of the thin films, θ is the angle of the peak and λ is the wavelength of the X-ray. The full width at half maximum (FWHM), which is the width of the peak at half the maximum peak intensity, is inversely proportional to the crystal size and is related to the degree of crystallinity in columnar polycrystalline thin films [30]. Fig. 2 shows the FWHM values at 2θ of the (1 0 2) diffraction peak for the samples with 1, 2, 3 and 5 wt% AlF_3 and the (0 0 3) diffraction peak for the sample with 7 wt% AlF_3. The corresponding crystal sizes of the films are also plotted as a function of the AlF_3 concentration in Fig. 2. As shown in the figure, the film with 2 wt% AlF_3 concentration had the lowest FWHM value and thus the maximum crystal size.

XPS analyses demonstrated the atomic composition and the chemical binding states in AZO:F films; only zinc, aluminium, oxygen and fluorine appeared on the film surfaces. The position of the carbon 1s peak was taken as the standard (with a binding energy of 284.6 eV) to compensate for any charge-induced shifts. The binding energies obtained from the measurements agreed well with the values reported in the literature [31–34]. Figs. 3 and 4 show the XPS spectra of the Al 2p peak and the F 1s peak for the ZnO films doped with 2, 5 and 7 wt% AlF_3. Both aluminium and fluorine signals increased with AlF_3 concentration. As shown in Fig. 3, the peak located at 75.0 eV was attributed to the substitution of Al atoms in the ZnO crystal lattices, which indicated the formation of Al_2O_3 according to the XPS catalogue data [35]. Doping AlF_3 into the lattice of ZnO produced a small chemical signal for the binding energy of F 1s peak at the core level, as shown in Fig. 4. The peak located at 685.1 eV was a typical value for the binding energy of the F 1s peak at the core level in fluoride compounds.

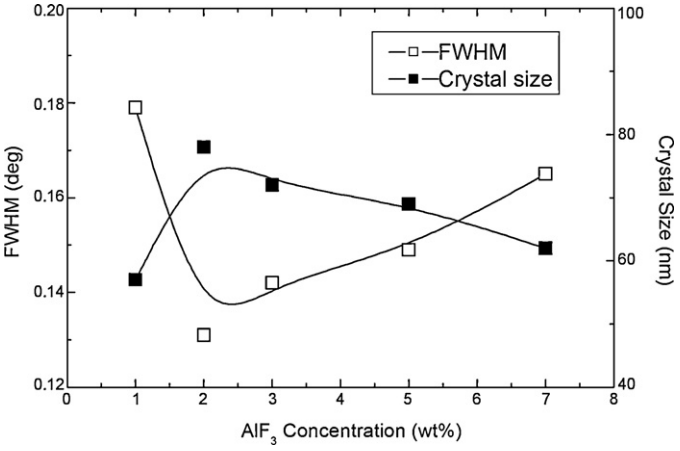

Fig. 2. FWHM and crystal size of ZnO film plotted as a function of AlF_3 concentration.

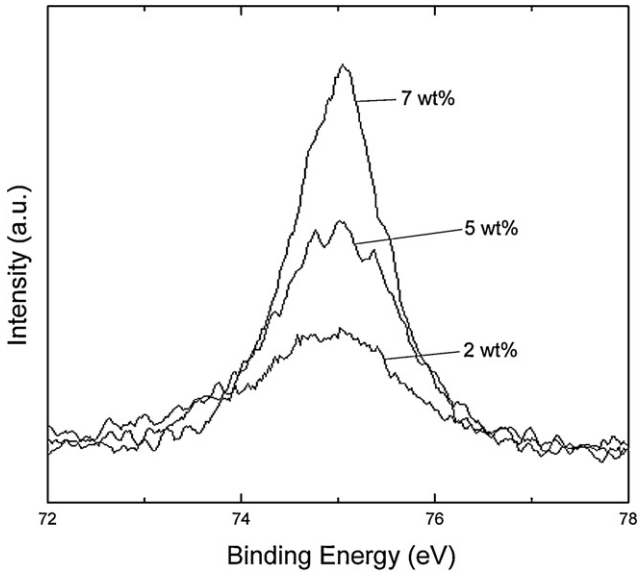

Fig. 3. XPS narrow scan in the aluminium 2p region for AZO:F films with AlF_3 concentrations at 2, 5 and 7 wt%.

FESEM images of the AZO:F films are shown in Fig. 5 with different AlF_3 concentrations deposited at an RF power of 70 W for 30 min. In the sample doped with 1 wt% AlF_3, the microstructure showed grains that were less homogeneously packed. The grain size was approximately 45 nm, which was comparable with the XRD results calculated based on the Scherrer formula. As the amount of AlF_3 increased, the film surface began to exhibit pyramidal morphology. The pyramidal surface texturing was due to the nucleation of oriented *c*-axis grains that grew geometrically and impinged each other laterally [36]. No obvious grain boundary characteristics were observed; the pyramid-like grains were 120 nm long and 50 nm wide. As the AlF_3 content increased to 7 wt%, distinct and independent grain morphology was observed; the grains were more regular and equiaxial in shape with an average grain size of approximately 65 nm.

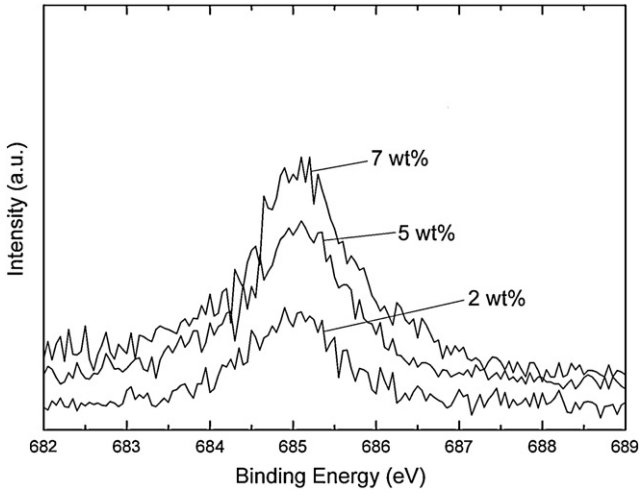

Fig. 4. XPS narrow scan in the fluorine 1s region for AZO:F films with AlF_3 concentrations at 2, 5 and 7 wt%.

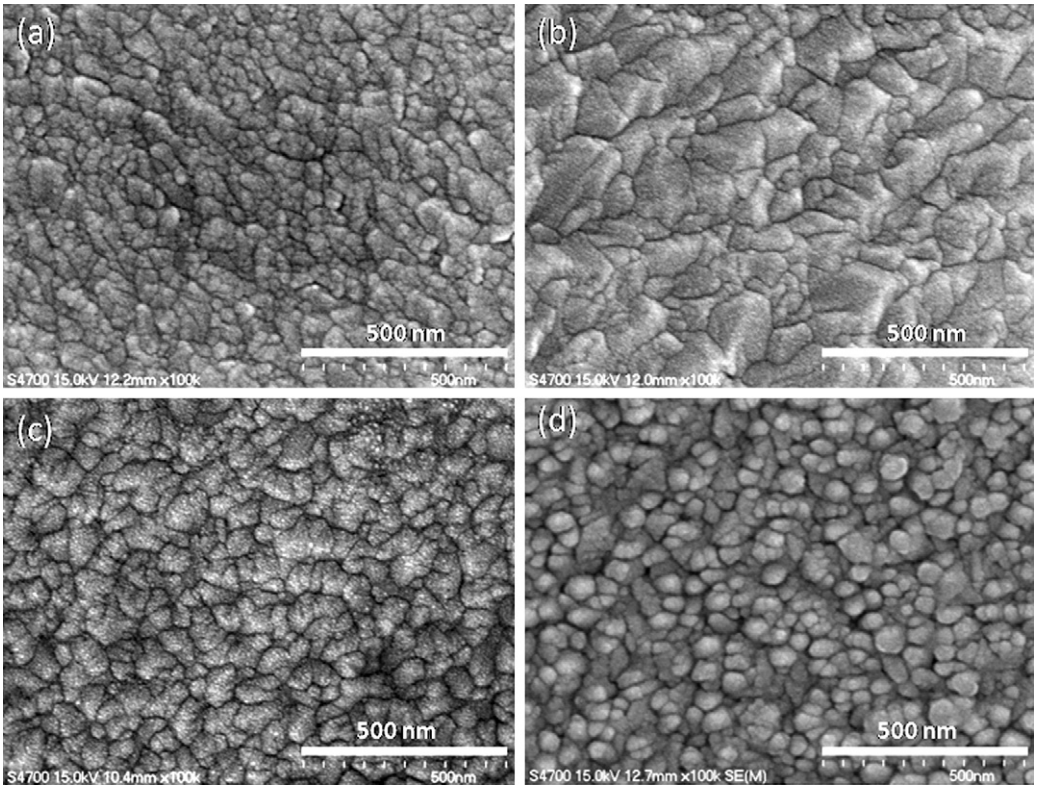

Fig. 5. FESEM images of AZO:F thin films with AlF_3 concentrations at (a) 1, (b) 2, (c) 5, and (d) 7 wt%.

The change in surface morphology of the ZnO with varying AlF_3 concentration could be seen in the AFM images shown in Fig. 6. The ZnO films prepared with higher AlF_3 concentrations were significantly rougher than those with lower AlF_3 concentration. The root mean square (Rms) roughness of the film was approximately 6.2 nm for the film with 1 wt% AlF_3 and increased up to 17.4 nm as the AlF_3 concentration increased to 7 wt%. The latter was a film with spherical-grains that were almost uniform in size and shape, but micro-pores were seen to spread around the grain boundary and resulted in a rougher film surface.

More detailed geometrical structure of the AZO:F films were observed by TEM. Fig. 7 is cross-sectional image of the ZnO film doped with 2 wt% AlF_3; the figure is associated with a selected-area diffraction (SAD) pattern on the upper right corner taken from the area shown in the TEM photography of Fig. 7(a). The observed microstructure of the film showed a dense and well-defined columnar morphology. Interestingly, the width of the columns was smaller near the substrate surface, while the ones on the top were larger and did not have obvious grain boundaries. This indicated that the films had competing growth mechanisms [37]. The SAD pattern was composed of a series of rings corresponding to the (0 0 2) and (1 0 3) planes. The SAD results further proved that these columns were indeed ZnO with the (0 0 2) plane being parallel to the substrate surface. Fig. 7(b) is a high resolution image of the lattice near the interface between two individual AZO:F columnar grains. It was also possible to see deformed lattice fringes and moiré patterns, implying the existence of some dislocations in the films.

3.2. Electrical and optical property evaluations

The electrical resistivity of AZO:F films produced at room temperature was plotted as a function of the AlF_3 concentration, and shown in Fig. 8. The data clearly indicated that the electrical resistivity of the films decreased to a minimum of $5.2 \times 10^{-4}\ \Omega\,\mathrm{cm}$ as AlF_3 concentration increased to 2 wt%. The decrease in resistivity was accompanied by an increase in the carrier concentration to $1.25 \times 10^{21}\ \mathrm{cm}^{-3}$, while the mobility was maximised approximately $9.3\ \mathrm{cm}^2\,\mathrm{V}^{-1}\,\mathrm{s}^{-1}$. The increase in electrical conductivity was mainly attributed to the improved crystallinity of the ZnO and the larger grain sizes as seen from the XRD and FESEM results. The dense microstructure contained fewer pores, which acted as traps for the free carriers and barriers for transporting the carrier in the film. Hence, the decrease in porosity was associated with the increase in grain size and the decrease in electron scattering, which led to the increase in conductivity.

The films with higher AlF_3 concentration showed a gradually increasing electrical resistivity as a result of the decrease in mobility, while the electron carrier concentration increased slightly and saturated. At a high AlF_3 concentration, the film contained high carrier concentrations due to the substitution of more electrically active Al and F atoms into the zinc and oxygen sub-lattice sites, respectively, thereby promoting more free electrons to the conduction band. On other hand, the effect of carrier mobility on the electrical conductivity of the thin films was more complex. Many sources of electron scattering centres can affect the carrier mobility of

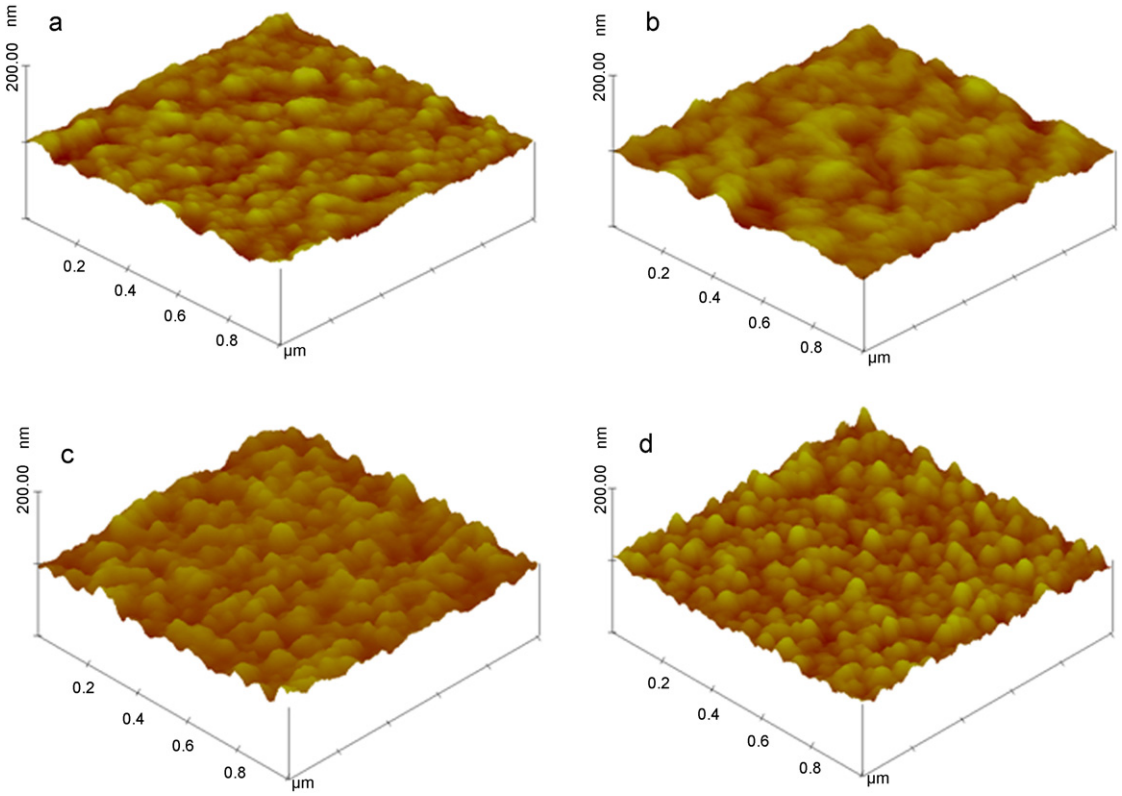

Fig. 6. AFM images of AZO:F thin films with AlF_3 concentrations at (a) 1, (b) 2, (c) 5, and (d) 7 wt%.

ZnO films [38–40]. In general, the reciprocal mobility of the films can be expressed as

$$\frac{1}{\mu_H} = \frac{1}{\mu_i} + \frac{1}{\mu_l} + \frac{1}{\mu_g} \tag{2}$$

where μ_H is the Hall mobility of the films, μ_i, μ_l, and μ_g are mobilities corresponding to the ionised impurity, lattice vibration and grain boundary scattering, respectively. At high temperatures, lattice vibration scattering may become dominant according to the equation $\mu_l \propto 1/T$ [41], indicating that the mobility of the film is inversely proportional to temperature. Because the films were deposited at approximately 25 °C, lattice vibration scattering did not play a significant role. Meanwhile, grain boundary scattering is considered another important scattering mechanism in polycrystalline semiconductor thin films [42–44]. However, scattering by grain boundaries in most cases is negligible because the mean free path length of the electrons is smaller than the crystallite size [11]. Therefore, ionised impurity scattering is considered the dominant and most appropriate mechanism in doped TCO films with a carrier concentration $>10^{20}$ cm^{-3}[18]. The impurities that cause the electron scattering include intrinsic lattice defects and extrinsic dopants. The calculated theoretical contribution to electrical conductivity due to ionised impurity scattering was evaluated by Conwell and Weisskopf [45] and Dingle [46]. Assuming these impurities are all ionised and, $n_e = N_i$, the

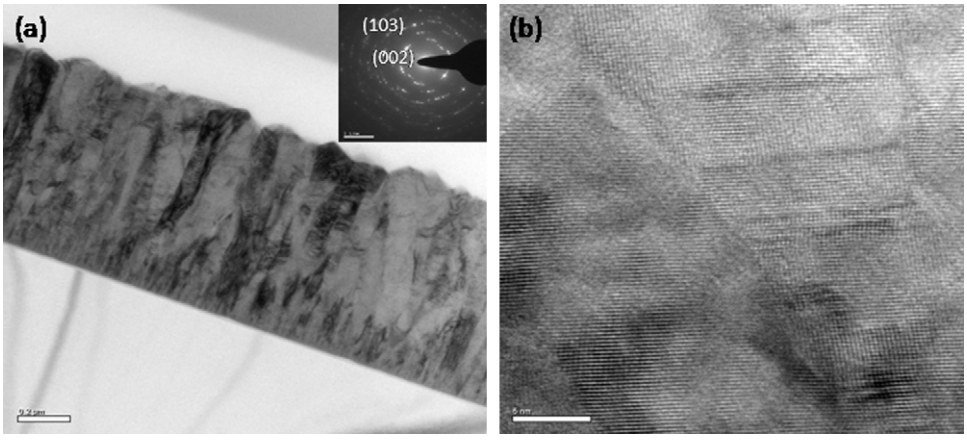

Fig. 7. TEM images of (a) the cross-section and the associated diffraction pattern for the ZnO film doped with 2 wt% AlF_3 deposited at room temperature, (b) two individual columnar grains of the sample presented from (a).

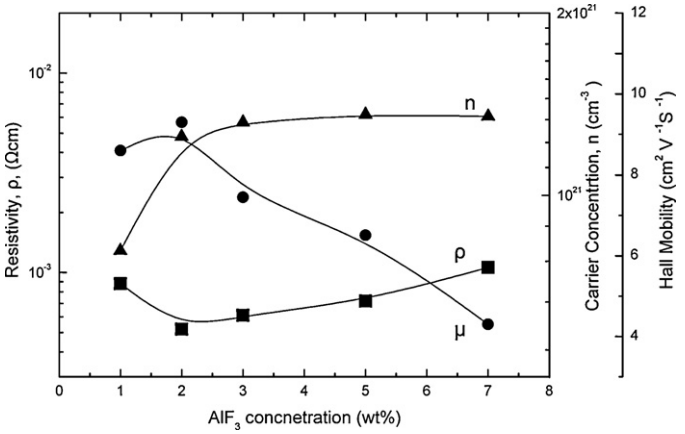

Fig. 8. Electrical resistivity, carrier concentration and mobility of AZO:F films as a function of AlF_3 concentration.

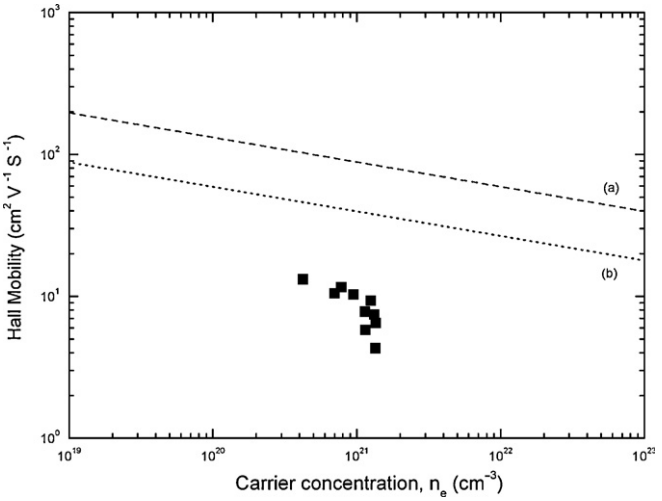

Fig. 9. The relationship between Hall mobility and carrier concentration of AZO:F films. The experimental data (filled square) and calculated mobilities are based on the ionised impurity scattering and the assumption that all the carriers are singly charge $Al_{Zn}^{\bullet}$ and $F_O^{\bullet}$ (line a) or oxygen vacancies $V_O^{\bullet\bullet}$ (line b).

mobility of highly degenerate TCO films, (μ_i), can be expressed as

$$\mu_i = \frac{24\pi^3(\varepsilon_0\varepsilon_\gamma)^2h^3n_e}{e^3m^{*2}g(x)z^2N_i} \tag{3}$$

where ε_0 and ε_γ are the permittivity of free space and low frequency of permittivity, respectively; n_e, m^*, z, and N_i are the electron concentration, the effective electron mass, the charge of the ionised centre, and the density of the ionised scattering centre, respectively. The $g(x)$ in the equation is the screening function given by:

$$g(x) = \ln\left(1+\frac{4}{x}\right) - \left(1+\frac{4}{x}\right)^{-1} \tag{4}$$

and

$$x = \frac{4e^2m^*}{4\pi\varepsilon_\gamma h^2(3\pi^5)^{1/3}n_e^{1/3}} \tag{5}$$

The limited mobility of ionised impurities, as calculated and described above, has been cited in many references that described the effect of charged scattering centres on the mobility of degenerate semiconductors [47,48]. Thus, the theoretical variation of μ_i with n_e was obtained by substituting the corresponding value of m^* with a maximum value of approximately $0.3m_e$ [49] and the value of ε_γ with 8.14 for ZnO [50]. Fig. 9 is a plot of the experimental values of μ_H as a function of n_e for the AZO:F films. The figure also shows the theoretical calculations of μ_i based on Eq. (3) against an electron concentration of n_e assuming that the mobility was entirely due to singly charged $Al_{Zn}^{\bullet}$ and $F_O^{\bullet}$ (line a) or oxygen vacancies, $V_O^{\bullet\bullet}$(line b). It is known that the electrical properties of ZnO film can be regulated by simultaneously substituting generic donor atoms (such as Al) into Zn and F into O lattice sites. In this work, AlF_3 was selected as a doping source; thus, the chemical reaction for the defect took place according to the following reaction [51]:

$$AlF_3 \xrightarrow{Zno} Alzn^{\bullet} + 3F_O^{\bullet} + 4e' \tag{6}$$

The defect reaction could also be originated from intrinsic defects of oxygen vacancies according to the following defect reaction:

$$O_O \rightarrow V_O^{\bullet\bullet} + \frac{1}{2}O_2 + 2e' \tag{7}$$

where $Al_{Zn}^{\bullet}$ and $F_O^{\bullet}$ represent the aluminium and fluorine ions on zinc and oxygen sites, respectively; O_o is an oxygen ion on an oxygen site, $V_O^{\bullet\bullet}$ is the vacant oxygen site, and e' is an electron in the conduction band. It was essential that the scattering caused by doubly charged oxygen vacancies ($V_O^{\bullet\bullet}$)) was greater than the scattering caused by singly charged $Al_{Zn}^{\bullet}$ or $F_O^{\bullet}$ because the values of n_e/z^2N_i for $Al_{Zn}^{\bullet}$ or $F_O^{\bullet}$ were 1 and 0.5, respectively according to Eq. (3). All experimental data points in this plot were right below the straight lines due to the double impacts on ionised impurity scattering by simultaneously substituting Al and F atoms into ZnO crystal lattices through AlF_3 doping. For the purpose of comparison, the data from ZnO films doped with Al_2O_3 were also presented. The data showed less deviation from the theoretical line because only the Al element substituted into the Zn lattice sites, which resulted in less ionic impurity scattering and a higher mobility.

The electrical properties of the sample doped with Al_2O_3 were also measured and compared to those of samples doped with AlF_3. Table 1 lists the electrical resistivity, carrier concentration and mobility of the ZnO films doped 2 wt% AlF_3 and Al_2O_3. It was clear that the electrical resistivity of the sample doped with AlF_3 was lower than that of the sample doped with Al_2O_3. Doping the film with AlF_3 not only provided cationic Al ions to substitute into Zn sub-lattice sites, but it also provided anionic F ions to substitute into O sub-lattice sites and resulted in a higher carrier concentration. However, more simultaneous doping opportunities from Al and F atoms might also cause more dopant impurities to reside on grain boundaries or interstitials. The dopant impurities acted as obstacles for the free carriers and reduced the carrier mobility. As seen in Table

Table 1
Comparison between the electrical properties of Al_2O_3- and AlF_3-doped ZnO films.

2 wt%	ρ (Ω cm)	n ($\times 10^{21}$ cm^{-3})	μ (cm^2 V^{-1} s^{-1})
AlF_3	5.2	1.25	9.3
Al_2O_3	6.4	0.86	11.2

1, the sample doped with AlF_3 had a lower carrier mobility (9.3 cm^2 V^{-1} s^{-1}) than the sample doped with Al_2O_3 (11.2 cm^2 V^{-1} s^{-1}) despite the higher carrier concentrations in the AlF_3-doped sample. Fig. 10 shows the variation in electrical resistivity of the ZnO films doped with AlF_3 and Al_2O_3 as a function of dopant concentrations. It is interesting to note that the window of dopant concentration that produced ZnO film with a low resistivity was narrower with AlF_3 as a dopant (2–3 wt%) than with Al_2O_3 as a dopant (2–5 wt%). This might also be related to the double doping effects of AlF_3, which provided the cationic Al and anionic F ions. That is, a small amount of AlF_3 would be required to obtain the same amount of free carriers as Al_2O_3 because only Al ion would substitute Zn sub-lattice sites.

The optical transmission spectra of the AZO:F films deposited at room temperature are shown in Fig. 11. The average optical transmissions of the samples doped with AlF_3 from 1 to 7 wt% were greater than 80% in the visible range. However, the film prepared at 7 wt% showed the lowest transmittance. This variation could be related to the film structure. As seen from the FESEM and AFM results, the microstructure of the film contained porosities associated with a rougher surface that led to more light scatterings and thereby a low transmittance in the visible region.

The local maximum and minimum transmittance ranged from 500 to 900 nm. These oscillations in the optical transmission spectra were attributed to the thickness of the film and to the interference between the ZnO/substrate interfaces. The most significant difference in the transmittance

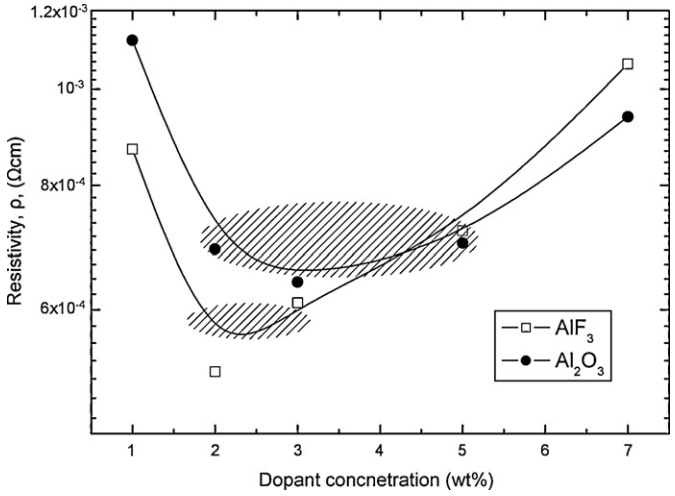

Fig. 10. Electrical resistivities of ZnO films doped with Al_2O_3 and AlF_3 as a function of dopant concentration.

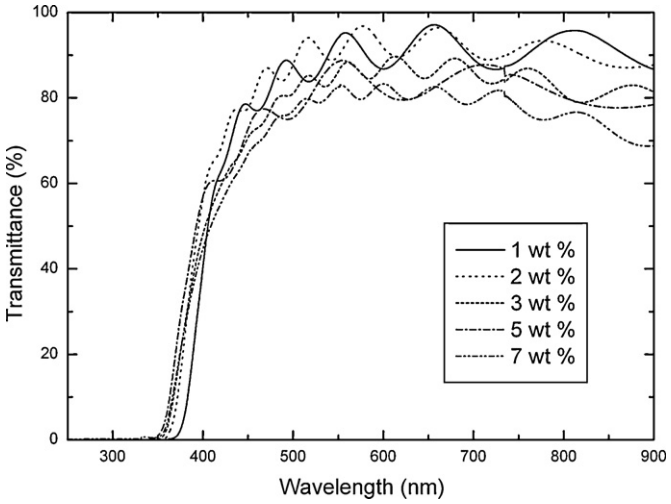

Fig. 11. Optical transmittance spectra of AZO:F films produced at different AlF_3 concentrations.

curves of the materials was in the threshold of optical absorption. Namely, the threshold of AlF_3-doped ZnO films was shifted to shorter wavelengths; thus, the band gap increased due to an increase in the carrier concentration of the film. The optical properties of ZnO films were related to the free carrier absorption and could be expressed by the Drude theory [52]. Using the transmittance and reflectance data, the absorption coefficient (α) of the films was calculated according to the following expression:

$$I = I_0 e^{-\alpha d} \tag{8}$$

where I is the intensity of the transmitted light, I_0 is the intensity of the incident light and d is the thickness of the film. Using the following relationship, the absorption coefficient data were used to determine the energy gap (E_g):

$$\alpha h\nu \approx (h\nu - E_g)^{1/2} \tag{9}$$

where $h\nu$ is the photon energy. In Fig. 12, α^2 was plotted against the photon energy of the films shown in Fig. 10. The values of the direct optical band gap, E_g, were determined by extrapolating the linear region of the plots to zero absorption. The results suggested that the direct band gap of the ZnO film doped with 1 wt% AlF_3 was 3.332 eV, while the direct band gap of the film doped with 2–7 wt% AlF_3 was 3.350–3.394 eV. The observed widening of the band gap was attributed to a Burstin–Moss shift [53,54]. According to the Burstin–Moss theory, the lowest states of the conduction band are occupied by free electrons, and valence electrons require extra energy to be excited to higher energy states within the conduction band. Therefore, the optical band gaps of the films prepared at high AlF_3 doping concentrations were wider than that of the film doped with 1 wt% AlF_3. Indeed, the optical spectra verified the Hall measurements and suggested that the carrier concentrations for the ZnO films prepared at high AlF_3 doping concentration were greater than that for the film doped with 1 wt% AlF_3.

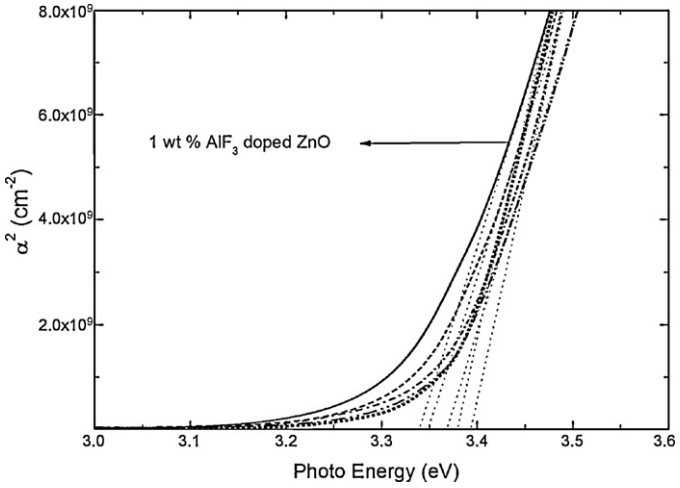

Fig. 12. Square of the absorption coefficient, α^2, plotted against photon energy as a function of AlF_3 concentration corresponding to the samples in Fig. 11.

4. Conclusions

AlF_3 was selected as the dopant source for ZnO thin films that were prepared at room temperature by RF magnetron sputtering. The variation of AlF_3 concentrations on the microstructure, electrical and optical properties of ZnO films were examined. It was found that the ZnO film doped with 2 wt% AlF_3 showed a highly oriented crystalline structure in the (0 0 2) direction. The microstructure also revealed a competing growth mechanism characterised by pyramid-like grains that were 120 nm long and 50 nm wide. As the AlF_3 content increased further, the size of the pyramid-like grains started to decrease and finally became regular and equiaxial in shape with an average grain size approximately 65 nm at 7 wt% AlF_3.

The ZnO film doped with 2 wt% AlF_3 had a minimum electrical resistivity of approximately $5.2 \times 10^{-4}\ \Omega$ cm with a carrier concentration of $12.5 \times 10^{20}\ cm^{-3}$ and a mobility of $9.3\ cm^2\ V^{-1}\ s^{-1}$. The improvement in electrical conductivity was attributed to improved crystallization and large grain size. However, the relative low mobilities were limited by ionised impurity and grain boundary scatterings, especially at higher AlF_3 concentrations. In comparison to the ZnO film doped with 2 wt% Al_2O_3, the AlF_3-doped film had a lower electrical resistivity in terms of carrier concentration enhancement. This is due to the double doping effects from the cationic Al and anionic F ions that simultaneously substituted into the Zn and O sublattice sites, respectively. However, the substitution also led to a lower carrier mobility because of increased scattering due to impurities.

The optical transmittance spectra in the visible region of the AlF_3-doped ZnO films at different AlF_3 doping levels were all higher than 80%. The band gap of the films was calculated and the values were within the range of 3.332–3.394 eV. The observed widening of the band gap was attributed to a Burstin–Moss shift. The optical spectra verified the Hall measurements and suggested that the carrier concentrations of the ZnO films doped at higher AlF_3 contents were greater than that of the ZnO films doped with 1 wt% AlF_3.

Acknowledgement

The authors are grateful for the financial support from the National Science Council of Taiwan (Grant No. 99-2221-E-214-009).

References

[1] K.S. Weibenrieder, J. Muller, Conductivity model for sputtered ZnO-thin film gas sensors, Thin Solid Films 30 (1997) 30–41.
[2] E. Olsson, L.K.L. Falk, G.L. Dunlop, R. Osterlund, The microstructure of a ZnO varistor material, J. Mater. Sci. 20 (1985) 4091–4098.
[3] C.R. Gorla, N.W. Emanetoglu, S. Liang, W.E. Mayo, Y. Lu, M. Wraback, H. Shen, Structural, optical, and surface acoustic wave properties of epitaxial ZnO films grown on (0 1 1 2) sapphire by metalorganic chemical vapor deposition, J. Appl. Phys. 85 (1999) 2595–2602.
[4] M.H. Koch, P.Y. Timbrell, R.N. Lamb, The influence of film crystallinity on the coupling efficiency of ZnO optical modulator waveguides, Semicond. Sci. Technol. 10 (1995) 1523–1527.
[5] D.C. Look, D.C. Reynolds, C.W. Litton, R.L. Jones, D.B. Easton, G. Cantwell, Characterizaton of homoepitixal P-type ZnO grown by molecular beam epitaxy, Appl. Phys. Lett. 81 (2002) 1830–1833.
[6] G. Hass, J. Heaney, A.R. Toft, Transparent electrically conducting thin films for spacecraft temperature control applications, Appl. Opt. 18 (1975) 1488–1489.
[7] R. Barber, G. Pryor, E. Reinheimer, Designing for electromagnetic compatibility, in: SID, Digest of Tech., vol. 28, 1997, p. 18.
[8] G. Sberveglieri, B. Benussi, G. Coccoli, S. Groppelli, P. Nelli, Thin films as NO and NO_2 gas sensors, Thin Solid Films 186 (1990) 349–360.
[9] C. Grivas, S. Mailis, L. Boutsikaris, D.S. Gill, N.A. Vainos, P.J. Chandler, Growth and performance of pulsed laser deposited indium oxide thin-film holographic recorders, Laser Phys. 8 (1998) 326–330.
[10] B.G. Choi, I.H. Kim, D.H. Kim, K.S. Lee, T.S. Lee, B. Cheong, Y.J. Baik, W.M. Kim, Electrical, optical and structural properties of transparent and conducting ZnO thin films doped with Al and F by RF magnetron sputter, J. Eur. Ceram. Soc. 25 (2005) 2161–2165.
[11] R.B.H. Tahar, T. Ban, Y. Ohya, Y. Takahashi, Tin doped indium oxide thin films: electrical properties, J. Appl. Phys. 83 (1998) 2631–2645.
[12] T. Minami, H. Sato, H. Nanto, S. Takata, Group III impurity doped zinc oxide thin films prepared by RF magnetron sputtering, Jpn. J. Appl. Phys. 24 (1985) L781–L784.
[13] D.C. Look, D.C. Reynolds, J.R. Sizelove, R.L. Jones, C.W. Litton, G. Cantwell, W.C. Harsch, Electrical properties of bulk ZnO, Solid State Commun. 105 (1998) 399–401.
[14] K. Tominaga, N. Umezu, I. Mori, T. Ushiro, T. Moriga, I. Nakabayashi, Transparent conductive ZnO film preparation by alternative sputtering of ZnO:Al target and either Zn or Al targets, Thin Solid Films 334 (1998) 35–39.
[15] I.A. Rauf, Extraction of free carrier density and mobility from the optical transmission data of tin-doped indium oxide thin films, Mater. Lett. 18 (1993) 123–127.
[16] K. Ellmer, Resistivity of polycrystalline zinc oxide films: current status and physical limit, J. Phys. D Appl. Phys. 34 (2001) 3097–3108.
[17] T. Minami, Y. Takada, S. Takata, T. Kakumu, Preparation of transparent conducting $In_4Sn_3O_{12}$ thin films by DC magnetron sputtering, Thin Solid Films 308 (1997) 13–18.
[18] J.M. Philips, J. Kwo, G.A. Thomas, A.S. Carter, R.J. Cava, S.Y. Hou, J.J. Krajewski, J.H. Marshall, W.F. Peck, D.H. Rapkine, R.B. van Dover, Transparent conducting thin films of $GaInO_3$, Appl. Phys. Lett. 65 (1994) 115–117.
[19] G.B. Palmer, K.R. Poeppelmeier, Conductivity and transparency of ZnO/SnO_2 co-substituted In_2O_3, Chem. Mater. 9 (1997) 3121–3126.
[20] S. Suzuki, T. Miyata, M. Ishii, T. Minami, Transparent conducting V co-doped AZO thin films prepared by magnetron sputtering, Thin Solid Films 434 (2003) 14–19.

[21] H.T. Cao, Z.L. Pei, J. Gong, C. Sun, R.F. Huang, L.S. Wen, Transparent conductive Al and Mn doped ZnO thin films prepared by DC reactive magnetron sputtering, Surf. Coat. Technol. 184 (2004) 84–92.
[22] T. Minami, S. Suzuki, T. Miyata, Transparent conducting impurity co doped ZnO:Al thin films prepared by magnetron sputtering, Thin Solid Films 398–399 (2001) 53–58.
[23] B. Houng, C.S. Hsi, B.Y. Hou, S.L. Fu, Fabrication and properties evaluation of aluminum and ruthenium co-doped zinc oxide thin films, J. Alloys Compd. 456 (2008) 64–71.
[24] K. Tominaga, T. Takao, Fukushima, T. Moriga, Nakabayashi, Film properties of ZnO:Al contaminated Zn targets with Co, Mn and Cr, Vacuum 66 (2002) 511–515.
[25] N. Fujimura, T. Nishihara, S. Goto, J. Xu, T. Ito, Control of preferred orientation for ZnO_x films: control of self-texture, J. Cryst. Growth 130 (1993) 269–279.
[26] C.R. Aita, A.J. Purdes, R.J. Lad, P.D. Funkenbusch, The effect of O_2 on reactively sputtered zinc oxide, J. Appl. Phys. 51 (1980) 5533–5536.
[27] Handbook of Chemistry and Physics, 67th ed., CNRS, Paris, 1986–1987.
[28] M. de la, L. Olvera, A. Maldonado, R. Asomoza, ZnO:F thin films deposited by chemical spray: effect of the fluorine concentration in the starting solution, Sol. Energy Mater. Sol. Cells 73 (2002) 425–433.
[29] B. Cullity, Elements of X-Ray Diffraction, Addison-Wesley, 1978, p. 102.
[30] H. Kim, C.M. Gilmor, Electrical, optical, and structural properties of indium-tin-oxide thin films for organic light-emitting devices, J. Appl. Phys. 86 (1999) 6451–6461.
[31] O. Bose, E. Kemnitz, A. Lippitz, W.E.S. Unger, XPS analysis of β-AlF3 phases with Al successively substituted by Mg to be used for heterogeneously catalyzed Cl/F exchange reactions, Appl. Surf. Sci. 120 (1997) 181–190.
[32] G. Moretti, G. Ferraris, G. Fierro, M. Lo Jacono, An XPS study of the reduction process of $CuO–ZnO–Al_2O_3$ catalysts obtained from hydroxycarbonate precursors, Surf. Interface Anal. 35 (2006) 224–228.
[33] G.E. Hammer, R.M. Shermenski, The oxidation of zinc in air studied by XPS and AES, J. Vac. Sci. Technol. A 2 (1983) 1026–1028.
[34] H.Y. Xu, Y.C. Liu, J.G. Ma, Y.M. Lou, Y.M. Lu, D.Z. Shen, J.Y. Zhang, X.W. Fan, R. Mu, Photoluminescence of F-passivated ZnO nanocrystalline films made from thermally oxidized ZnF_2 films, J. Phys. Condens. Matter 86 (2004) 5143–5150.
[35] G.D. Wagner, W.M. Riggs, L.E. Davis, J.F. Moulder, G.E. Mullenber, Handbook of X-Ray Photoelectron Spectroscopy, Perkin Elmer Corp., MN, 1992.
[36] P.M. Verghese, D.R. Clake, Surface textured zinc oxide films, J. Mater. Res. 14 (1999) 039–1045.
[37] J.F. Chang, C.C. Shen, M.H. Hon, Growth characteristics and residual stress of RF magnetron sputtered ZnO:Al films, Ceram. Int. 29 (2003) 245–250.
[38] J.R. Bellingham, W.A. Phillips, C.J. Adkins, Intrinsic performance limits in transparent conducting oxides, J. Mater. Sci. Lett. 11 (1992) 263–265.
[39] A.V. Singh, R.M. Mehra, Doping mechanism in aluminum doped zinc oxide films, J. Appl. Phys. 95 (2004) 3640–3643.
[40] D.H. Zhang, H.L. Ma, Scattering mechanisms of charge carriers in transparent conducting oxide film, Appl. Phys. A 62 (1996) 487–492.
[41] P.S. Kireev, Semiconductor Physics, Mir, Moscow, 1978.
[42] J.E. Morris, M.I. Ridge, C.A. Bishop, R.P. Howson, Temperature dependence of hall mobility in indium–tin oxide thin films, J. Appl. Phys. 51 (1980) 1847.
[43] S. Chaudhuri, J. Bhattacharyya, A.K. Pal, Microstructure of indium tin oxide films produced by the D.C. sputtering technique, Thin Solid Films 148 (1987) 279–284.
[44] M. Mizuhashi, Lamellar and grain boundary models for the electrical properties of post-oxidized ITO Films, Jpn. J. Appl. Phys. 1 22 (1983) 615–620.
[45] E. Conwell, V.F. Weisskopf, Theory of impurity scattering in semiconductors, Phys. Rev. 77 (1950) 388–390.
[46] R.B. Dingle, Scattering of electrons and holes by charged donors and acceptors in semiconductors, Philos. Mag. 46 (1955) 831–840.
[47] H. Bisht, H.T. Eun, A. Mehrtens, M.A. Aegerter, Comparison of spray pyolyzed FTO, ATO and ITO coating for flat and bent glass substrate, Thin Solid Films 351 (1999) 109–114.
[48] F.O. Adurodija, H. Izumi, T. Ishihara, H. Yoshioka, M. Motoyama, Effects of stress on the structure of indium–tin-oxide thin films grown by pulsed laser deposition, J. Appl. Phys. 88 (2000) 4175–4180.
[49] I. Hamberg, C.G. Grangvist, Evaporated Sn-doped In_2O_3 films: basic optical properties and applications to energy-efficient windows, J. Appl. Phys. 60 (1986) R123–R160.
[50] R.J. Collins, D.A. Kleinman, Infrared reflectivity of zinc oxide, J. Phys. Chem. Solids 11 (1959) 190–194.
[51] D.M. Smyth, The Defect Chemistry of Metal Oxides, Oxford University Press, 2000.
[52] H.L. Hartnagel, A.L. Dawar, A.K. Jain, C. Jagadish, Semiconducting Transparent Thin Films, Institute of Physics Publishing, Philadelphia, 1995.
[53] E. Burstein, Anomalous optical absorption limit in InSb, Phys. Rev. 93 (1954) 632–633.
[54] T.S. Moss, The interpretation of the properties of indium antimonide, Proc. Phys. Soc. B 67 (1964) 775–782.